A mathematical model to improve water storage of glacial lakes prediction towards addressing glacial lake outburst floods

Miaomiao Qi[a,b,c,d], Shiyin Liu[a,b,c]*, Zhifang Zhao[c,d]*, Yongpeng Gao[e,f], Fuming Xie[a,b], Georg Veh[g],

Letian Xiao[a,b], Jinlong Jing[h], Yu Zhu[a,b], Kunpeng Wu[a,b]

[a] *Yunnan Key Laboratory of International Rivers and Transboundary Eco-Security, 650091 Yunnan University, Kunming, China;*
[b] *Institute of International Rivers and Eco-Security, Yunnan University, 650091, Kunming, China;*
[c] *Yunnan International Joint Laboratory of China-Laos-Bangladesh-Myanmar Natural Resources Remote Sensing Monitoring, Kunming 650091, China;*
[d] *School of Earth Sciences, Yunnan University, Kunming 650500, China;*
[e] *Faculty of Geography, Yunnan Normal University, Kunming, 650500, China;*
[f] *Key Laboratory of Resources and Environmental Remote Sensing for Universities in Yunnan, Kunming 650500, China;*
[g] *Institute of Environmental Science and Geography, University of Potsdam, Potsdam, Germany*
[h] *School of Mathematics and Statistics, Yunnan University, 650091, Kunming, China;*

*Corresponding author: Shiyin Liu, shiyin.liu@ynu.edu.cn; Zhifang Zhao, zhaozhifang@ynu.edu.cn

Abstract: Moraine-dammed glacial lakes are vital sources of freshwater but also pose a hazard to mountain communities if they drain in sudden glacial lake outburst floods. Accurately measuring the water storage of these lakes is crucial to ensure sustainable use and safeguard mountain communities downstream. However, thousands of glacial lakes still lack a robust estimate of their water storages because bathymetric surveys in remote regions are difficult and expensive. Here we geometrically approximate the shape and depths of moraine-dammed lakes and provide a cost-effective model to improve lake water storage estimation. Our model uses the outline and the terrain surrounding a glacier lake as input data, assuming a parabolic lake bottom and constant hillslope angles. We validate our model using ten new bathymetrically surveyed glacial lakes on the Qinghai-Tibet Plateau, and compiled data from 34 recently measured lakes. Our model overcomes the autocorrelation issue inherent in earlier area/depth-water storage relationships and incorporates an automated calculation process based on the topography and geometrical parameters specific to moraine-dammed lakes. Compared to other models, our model achieved the lowest average relative error of approximately 14% when analyzing 44 observed data, surpassing the >44% average relative error from alternative models. Finally, the model is used to calculate the water storage change of

moraine-dammed lakes in the past 30 years in High Mountain Asia. The model has been proven to be robust and can be utilized to update the water storage of lake water for conducting further management of glacial lakes with the potential for outburst floods in the world.

1. Introduction

Moraine-dammed glacial lakes (MDLs) trap meltwater from snow, ice and liquid precipitation within basins behind dams at or near the termini of glaciers (Westoby et al., 2014; Yao et al., 2018; Veh et al., 2019). As glaciers have been retreating in past decades in most mountain regions worldwide, new MDLs have been forming, and existing ones have been growing in size and water storage (Bolch et al., 2012; Carrivick and Tweed, 2013; Cook et al., 2018; Shugar et al., 2020; Zhang et al., 2023). During the period from 1990 to 2018, High Mountain Asia witnessed a remarkable 52% and 54% increase in the number and area of MDLs, respectively (Wang et al., 2020). Notably, the Eastern Himalayas experienced the most significant growth, leading in both the number and area of MDLs during this period. MDLs are vital water reservoirs for communities in glaciated high mountains, but were also repeatedly sources for Glacial Lake Outburst Floods (GLOFs) (Westoby et al., 2014; Wu et al., 2019; Gao et al., 2021; Fischer et al., 2021; Zheng et al., 2021a). According to a report by Lützow et al. (2023), a total of 630 GLOFs have been linked to MDLs occurring in 27 countries between 850 and 2022 CE. A recent study indicates that multiple GLOFs documented from 1964 to 2022 have caused damage to infrastructure in High Mountain Asia (Nie et al., 2023).

MDLs are prone to sudden failure due to the instability of the dam structure, releasing parts of the impounded water storage in catastrophic floods (Westoby et al., 2014; Zheng et al., 2021b). MDLs can grow towards steep slopes, where debris or ice could fall into the lakes, causing the barriers to overflow (Emmer et al., 2014; Carrivick and Tweed, 2013; Liu et al., 2020). Due to their high altitude and potential energy, these flood waves can attain runout distances of many tens of kilometers, transporting and entraining large amounts of sediments from moraines and riverbanks (Westoby et al., 2014). Many GLOFs have transformed into debris flows and their coarse debris rapidly filled hydropower reservoirs and further destroyed infrastructure along the flow path (Westoby et al., 2014; Zheng et al., 2021b). For example, GLOFs descending from the mountains with high kinetic energy have recently damaged transport and power infrastructure such as the Upper Bhote Koshi hydropower plant, with a reconstruction cost of 57 million USD (United States dollar) (Cook et al., 2018). Future flash floods are a potential threat to major new infrastructure, for

example, hundreds more hydropower projects (Nie et al., 2023). GLOFs may also undercut hillslopes along mountain rivers, which may fail, impound river runoff, and form potentially unstable lakes (Zheng et al., 2021a). Thus, MDLs have become a major glacier-related hazard in high mountains, and will likely remain so as glaciers could lose more than a third of their mass by the end of the 21st century (Rounce et al., 2023). Appraising the water storage of glacial lakes is key to allowing for sustainable development along river channels originating in glaciated headwaters (Yao et al., 2018; Harrison et al., 2021; Shugar et al., 2020; Liu et al., 2020).

Effective management of GLOF hazards hinges on the ability to assess both the likelihood and magnitude of such events (Clague et al., 2000). This typically requires understanding several critical factors, including the water storage of MDL, the structural integrity and stability of the dam, potential external triggers, and the flood's anticipated flow path (e.g., Richardson and Reynolds, 2000; Westoby et al., 2014; Mergili et al., 2020; Sattar et al., 2021; Qi et al., 2023). Estimating glacial lake volume, however, presents significant challenges. Many glacial lakes are situated in remote, physically demanding, and hazardous environments, complicating bathymetric surveys of the lake basins (Cook and Quincey, 2015; Qi et al., 2022). Therefore, in situ measurements of lake depth are available only for a few dozen cases in the Himalayas, while the water storage remains unknown for the other thousands of lakes in this region. Current optical or radar-based satellite missions, while useful for mapping lakes, are limited in measuring lake bathymetry due to the strong attenuation of electromagnetic waves in glacial lakes (Zhu et al., 2019). As such, there has been an ongoing effort to refine empirical scaling relationships from the few available worldwide samples that relate glacial lake depth and/or area to lake water storage (Fujita et al., 2013; Loriaux and Casassa, 2013; Carrivick and Quincey, 2014; Cook and Quincey, 2015; Veh et al., 2019; Shugar et al., 2020; Qi et al., 2022). However, these equations may yield significant errors in orders of magnitude for a given lake area due to the the autocorrelation issue inherent in earlier area/depth-volume relationships. Although there are models considering the specific geometric shapes and topography surrounding lakes, they limited to estimating the water storage of larger size plateau tectonic lake (Zhou et al., 2020; Zhu et al., 2019). After numerous experiments, we have found that the aforementioned models do not apply to estimating the water storage of glacier lakes due to the lack of consideration for glacial lake and related parameters. Given the critical role of glacial lake water storage in assessing hazard risk and providing early warning information, the development of

96   a mathematically robust yet cost-effective model is urgently needed.

97   Our goal is to introduce a novel approach for accurately estimating water storage by

98   incorporating its geometry and surrounding terrain. To this end, we propose a three-dimensional

99   model to approximate the basin morphology of MDLs and derive its analytical equation. We assess

100 the performance of this model against field-measured underwater topography data and further

101 compare the model error against other available empirical scaling relationships. Finally, we discuss

102 the uncertainty and rationality of the new model and apply the model to estimate the water storage

103 of the MDLs in High Mountain Asia.

104 **2. MDLs types and their geometric approximation**

105 MDLs can be classified into glacier-contacted lakes (GCL) and glacier-uncontacted lakes

106 (GUL). GCLs are supraglacial ponds on top of debris-covered glaciers or lakes at the termini of

107 glaciers (Richardson 2000; Bennett et al., 2012). We term GCL as MDL in direct contact with the

108 glacier terminus (Figure 1a). By contrast, GULs are separated from the present glaciers, but

109 impound substantial parts of the meltwater from the glacier upstream (Figure 1b). The bottom of an

110 MDL may be a sediment-covered bedrock depression that was eroded and deepened by the parent

111 glacier during earlier advances. As glaciers retreat, they provide space for lakes to grow between

112 the glacier terminus, with the abandoned moraine trapping excess meltwater from the parent glacier

113 (Nie et al., 2023).
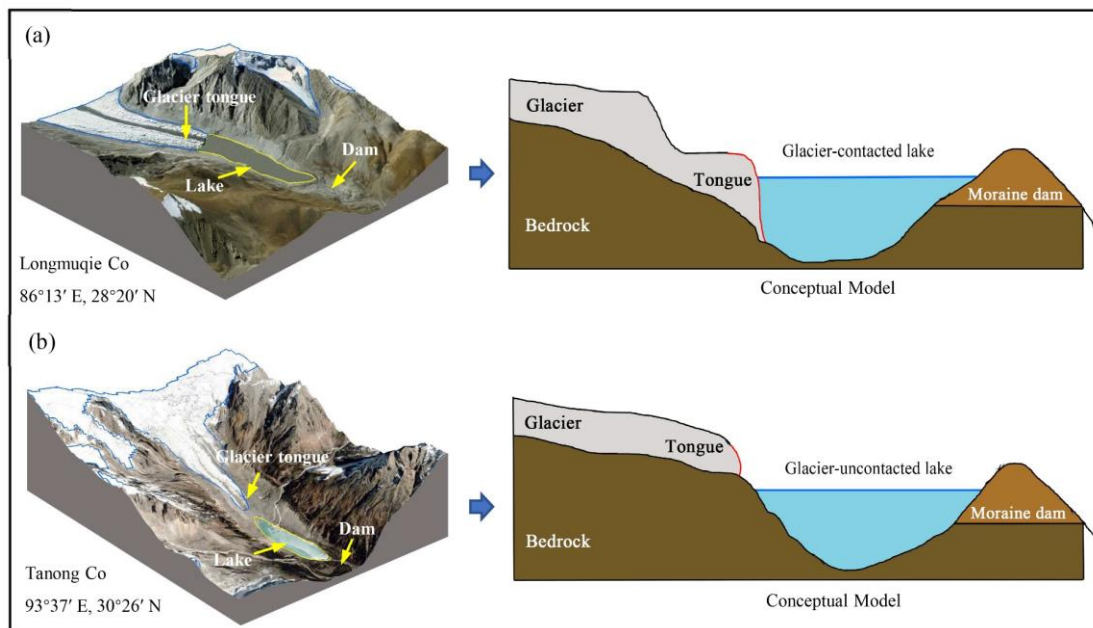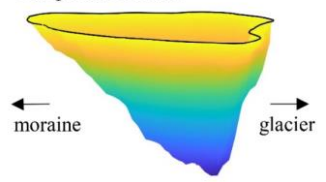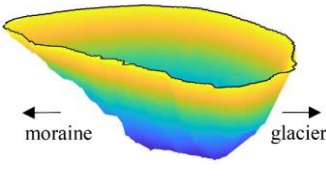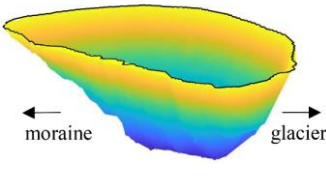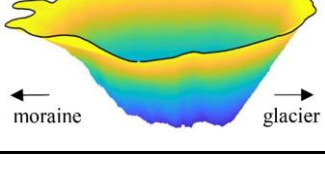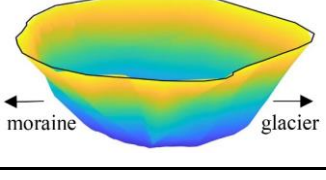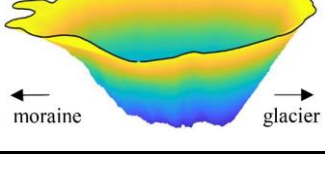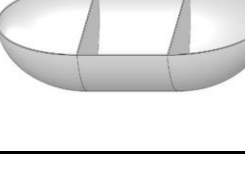
114

115 **Figure 1**. Longitudinal cross-sections along a glacier-contacted (a) and glacier-uncontacted lake (b) (The base

116 images are from Google Earth imagery) (©Google Earth). Sketches are idealized and do not represent measured

117 elevations.

118 We use the glacial lake inventory of High Mountain Asia by Wang et al. (2020) to differentiate

119 these two types of MDLs. In general, glacial lakes grow in area largely because they become longer.

120 Lower values of the ratio (R) between the maximum width and maximum length indicate that the

121 shape of the lake is elongated; R equals 1 if the lake is perfectly circular or square (Qi et al., 2022).

122 According to the glacial lake inventory, the R value for glacial lakes in High Mountain Asia ranges

123 from 0.1 to 1.0. If R is less than 0.1, it may indicate the presence of glacial lakes with lengths

124 exceeding 10 meters but widths of approximately 1 meter. However, in reality, glacial lakes with

125 such dimensions are practically non-existent. Therefore, thresholds of R allow us to distinguish

126 glacial lakes into four subclasses (Table 1). We find that newly formed GCLs typically have small

127 surface areas and high values of R. We classified GCLs with R between 0.70 ~ 1.0 as GCL-1, and

128 those with R less than 0.69 as GCL-2. Examples of these two types are Poiqu No.1 Lake (85.92°E,

129 28.14°N) and Bienong Co (93°26′E, 30°31′N) (Table 1). With ongoing glacier recession, lakes

130 might become decoupled from their parent glacier, switching from a lake-terminating to a land-

131 terminating glacier. We termed lakes as GUL-1, if R ranged between 0.5 and 1.0, and GUL-2 if $R <$

132 0.49. Paqu Co (86°15′E, 28°30′N) and Jialong Co in 2020 are the examples of these two classes

133 (Table 1). It is noteworthy that the establishment of the R threshold in this study is grounded in the

134 glacial lake catalog dataset developed by Wang et al, (2020). Initially, the glacial lakes were divided

135 into two major categories, GCL and GUL. Subsequently, R values for each glacial lake were

136 calculated, and all co-authors classified the geometric shapes based on different types and sizes of

137 glacial lakes. Ultimately, through statistical analysis of glacial lake sizes for different types, we

138 defined the threshold for R. This allows the model to automatically categorize glacial lakes based

139 on this value.

140 **Table 1** Examples of glacier-contacted lake and glacier-uncontacted lake. The ratio R represents the maximum width

141 (m) divided by the maximum length (m) of the glacial lake. The vertical scale is exaggerated.

Type	Lake bathymetry	Model	Features	R

GCL-1	PoiquNo.1 of 2021 ← moraine glacier →		A newly formed MDL typically has a small scale and is located at the glacier tongue.	0.70≤R≤1.0
GCL-2	Bienong Co of 2021 ← moraine glacier →		The MDL gradually grows in the area but has not yet reached the maximum range determined by the surrounding terrain.	0.10≤R≤0.69
GUL-1	Paqu Co of 2020 ← moraine glacier →		As the glacier continues to retreat, the distance between the glacier tongue and the MDL gradually increases.	0.50≤R≤1.0
GUL-2	Jialong Co of 2020 ← moraine glacier →		The length of the MDL increases with time due to the continuous supply with glacier meltwater.	0.10≤R≤0.49

3. Model Development

3.1. Input data

We suggest specific geometric models for the four subclasses (Table 1) to approximate the water storages of MDLs. Our models are fed with data from a digital elevation model (DEM) and from the outline of a glacial lake. We used a 12.5-meter ALOS PALSAR DEM, which is freely available from the Japan Aerospace Exploration Agency (JAXA, https://www.eorc.jaxa.jp).

3.2. Analytical equations

We surmise that an ideal cross-section of a MDL (Figure 2) can be partitioned into three distinct portions, V_1, V_2, and V_3, representing the water storage of the lake stored adjacent to the moraine dam, at the center of the lake, and near the glacier (or bedrock if the lake is disconnected from the glacier). The corresponding lengths of these three portions along the maximum length of the lake are denoted by m, r, and n. The lake has its maximum depth, h_1 and h_2, on either side of r. Points g and f represent the positions of a sediment layer at the lake bottom, and a and β are the slopes of

156   near the water surface.

157   The core assumptions of our geometric model can be summarized such that: 1) an MDL has a

158   parabolic longitudinal bottom profile with a uniform sediment layer at the bottom of the lake to keep

159    $h_1 = h_2$, and a parabolic cross-section P_S (Figs. 2; 3); (2) the lake surface shape can be approximated

160   by ellipses at both ends and a rectangle in between; (3) The glacier surface and the moraine dam dip

161   towards the lake with the same slope.

162

163
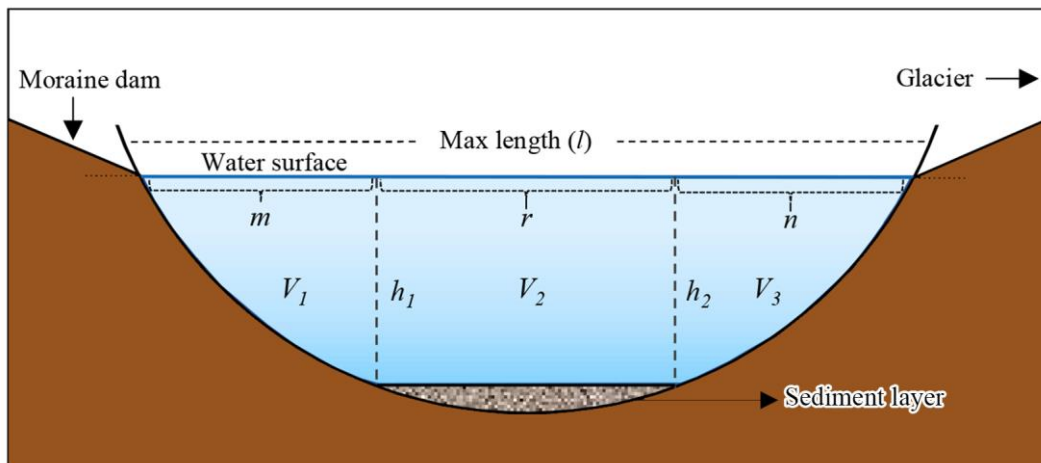
Figure 2. Longitudinal cross-section through a MDL. The blue horizontal line (l) is the maximum length on the lake
surface, subdivided by m, r, and n. The solid black line is the hypothetical bottom of the lake, and the gray texture
area represents a sediment layer covering the lake bottom. The maximum water depth is $h=h_1=h_2$, and points g and
f are at equal depths.

168   In three-dimensional form, the MDL basin can be divided into three parts with each having a

169   water storage of V_1, V_2, and V_3 (Figure 3a). V_1 and V_3 can be considered as the water storages of

170   elliptical semi-paraboloids controlled by the water depth h (Figure 3b and c). Significantly, V_1 and

171   V_3 may or may not be equal, depending on the values of m and n. V_2 is a semi-parabolic cylinder

172   (Figure 3d) that has height r, diameter w, and a parabolic cross-section P_s (Figure 3e). Thus, the total

173   water storage of the MDL is $V=V_1+V_2+V_3$.
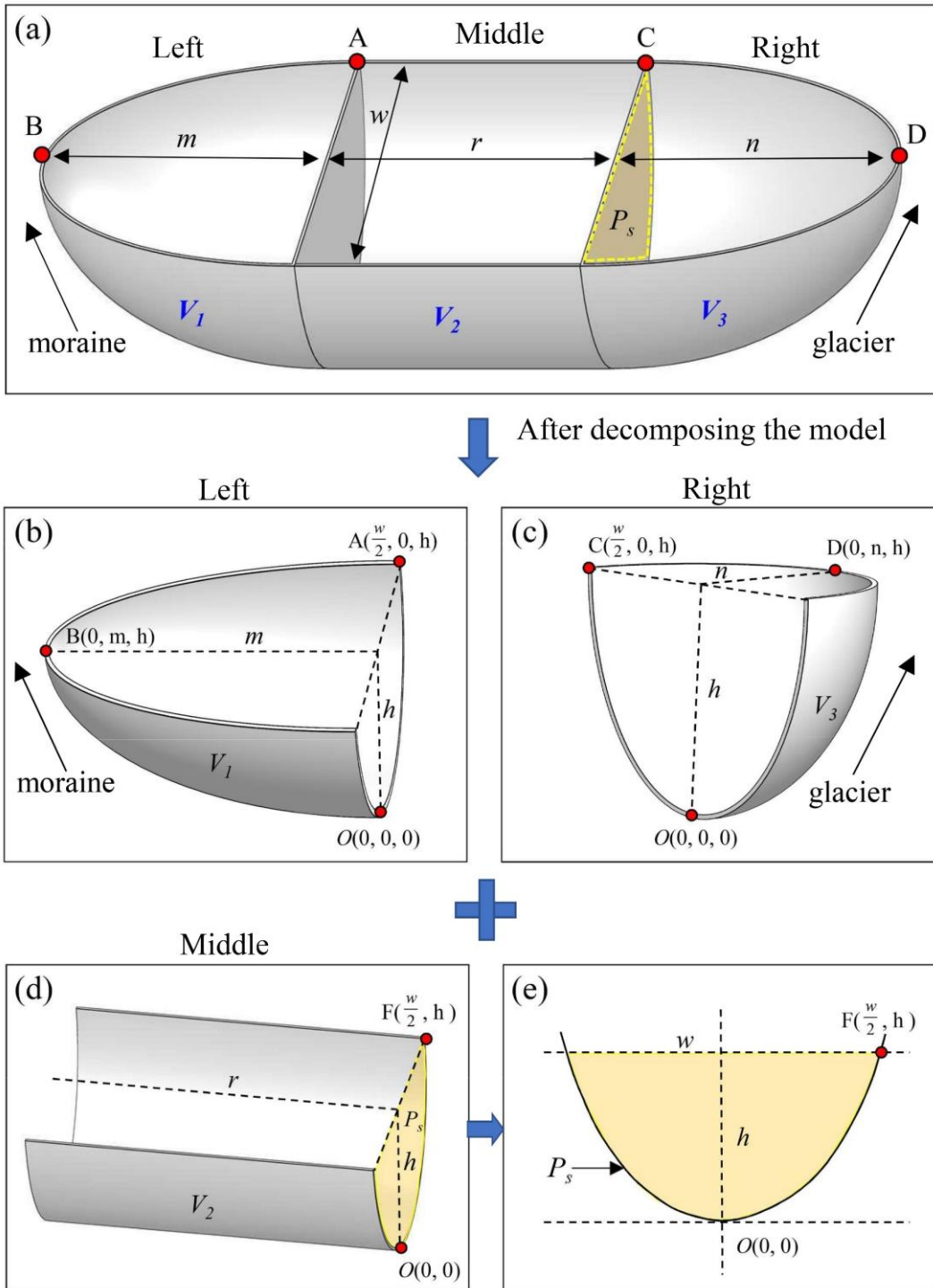
Figure 3. Definition diagram for the geometry of a MDL. a, hypothetical three-dimensional model of a MDL. b, Model for V_1 describing the lake water storage adjacent to the moraine dam. c, Model for V_1 describing the lake water storage adjacent to the glacier. d, Model for V_3 describing the lake water storage stored in the center part of the lake. e, Cross section of the column P_s. The parameters m and n are the semi-major axis of the elliptical paraboloid near the MDL inlet and outlet, respectively; r is the length of the parabolic cylinder in the middle of MDL; w and l represent the largest width and length of the MDL, respectively; h is the lake depth.

To obtain the individual lake water storages, we define the elliptical paraboloids for V1 and V2

(equations 1-2) in a Cartesian coordinate system (x, y, z) as

184
$$V_1 = \left\{ (x, y, z) \mid \frac{x^2}{a_1{}^2} + \frac{y^2}{b_1{}^2} \le z, y \ge 0, 0 \le z \le h \right\} \tag{1}$$

185
$$V_3 = \left\{ (x, y, z) \mid \frac{x^2}{a_2{}^2} + \frac{y^2}{b_2{}^2} \le z, y \ge 0, 0 \le z \le h \right\} \tag{2}$$

186 and the parabolic cylinder for V2 (equation 3) as

187
$$V_2 = \left\{ (x, y, z) \mid kx^2 \le z \le h, 0 \le y \le r \right\} \tag{3}$$

188 where $a_1 > 0$, $b_1 > 0$, $a_2 > 0$, $b_2 > 0$ are length of the semi-axes of upper surfaces of V_1 and V_3; $h >$

189 0 is the height of V_1, V_2 and V_3; $r > 0$ is the length of V_2.

190 Considering the four types of MDLs, GCL-1 corresponds to the case where $r=0$ and $n=0$. In

191 this study, m represents the part of the lake area closer to the moraine dam, and in most cases, m is

192 not equal to zero. However, in certain special cases, such as the Lake Zhasuo Co (93.25°E, 30.31°N)

193 in southeastern Tibet, $m=n=0$, because the surface morphology of this lake is rectangular. In most

194 scenarios, the water storage of the GCL-1 can be represented as:

195
$$V_{\text{GCL1}} = \frac{\pi wmh}{8}. \tag{4}$$

196 When $n=0$, the model of MDL corresponds to GCL-2, and its water storage can be

197 represented as

198
$$V_{\text{GCL2}} = \frac{\pi wmh}{8} + \frac{2}{3} whr. \tag{5}$$

199 When $r=0$, the model of MDL conforms to GUL-1, and its water storage can be expressed as:

200
$$V_{\text{GUL1}} = \frac{\pi whl}{4}. \tag{6}$$

201 When the type of MDL corresponds to GUL-2, its water storage can be expressed as:

202
$$V_{\text{GUL2}} = \frac{\pi wh(l-r)}{4} + \frac{2}{3} whr. \tag{7}$$

203 Finally, the water depth (h) can be derived from the w and slope angles (a) of the glacial lake:

204
$$h = \frac{w \tan(\alpha)}{4}. \tag{8}$$

205 Section 1 in the Supplementary file elaborates more on the derivation of these analytical

206 equations, Table 2 shows the definition of the abbreviations in the model procedure.

207 **Table 2**. The definition of the abbreviations in the geometric model.

Abbreviation	Description and definition

MDL	The moraine-dammed lake
GUL	The glacier-uncontacted lake
GCL	The glacier-contacted lake
R	The ratio of the maximum width to the maximum length of the MDL
m	The semi-major axis of the elliptical paraboloid of the MDL outlet
n	The semi-major axis of the elliptical paraboloid at the MDL inlet
c	The arbitrary height of the cross-section of an elliptic paraboloid
r	The length of the parabolic cylinder in the middle of MDL
h	The maximum water depth of MDL
w	The diameter of the largest inscribed circle of the MDL
l	The length of the minimum bounding rectangle of MDL
P_s	The cross-section of the middle of MDL
S_{Ps}	The area of the cross-section in the middle of MDL
a	The median slope of the 80 m buffer zone around the MDL

3.3. Determination of model parameters

We determined the parameters in Eq. 4 - 8, namely w, l, a, m, n and r, using the lake boundary and the DEM. We measured w and l by drawing a minimum rectangle bounding box with length l encompassing the MDL (Figure 4a). If the width w' of the bounding box of the MDL exceeds the actual width (w) of the lake, as in the case of the tortuous boundary of Lake Longmuqie Co (86.23°E, 28.35°N) (Figure 4b), we assign the diameter of the maximum inscribed circle within the MDL as w in Figure 4c.
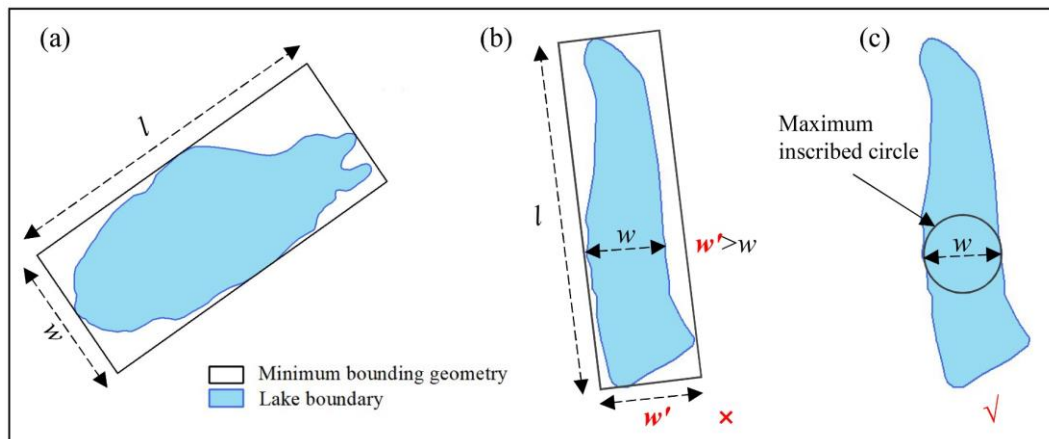
Figure 4 Schematic illustration of the method for extracting the maximum length (l) and width (w) of the MDL. The

217   outline in Figure a represents the geometric boundary of Lake Jialong Co (86.85°E, 28.21°N), while the outlines in

218   Figures b and c depict the geometric boundaries of Lake Longmuqie Co (86.23°E, 28.35°N).

219   To determine the slope a-value surrounding the MDL, we use a DEM with a spatial resolution

220   of 12.5 m in the model computation. We tested buffer sizes of 30 m, 50 m, 80 m, and 100 m width

221   beyond the MDL boundary, and extracted the mean and median value of a within each buffer. By

222   comparing the simulated results with the measured data (lakes Bienong Co, Maqiong Co, Tanong

223   Co, and Jialong Co), we found that the water storage estimation using the median value of a within

224   80 m external buffer zone had a lower relative error and higher overall accuracy. Therefore, we

225   defined a-value as the median slope within the 80 m buffer zone surrounding the MDL boundary.

226   The choice of buffer zone distance can be adjusted based on the specific terrain characteristics of

227   the research area, allowing researchers to adapt the methodology to their data accuracy.

228   Determining the appropriate thresholds for m, n, and r of different MDL types is challenging

229   as methods for extracting these parameters vary depending on the MDL types. In other words, due

230   to the different types of glacial lakes, the values of m, n, and r vary. Additionally, these values change

231   with the size of the glacial lake. To enable the model to automatically identify and calculate the

232   corresponding m, n, and r for each glacial lake, we need to define a threshold. Based on the geometry

233   of the glacial lake, we established a proportional relationship between m, n, r, and the glacier lake

234   length (l). This proportional relationship is empirically defined and essentially represents a

235   geometric segmentation of the glacial lake. The lake is divided into three sections, and the volume

236   of each section is calculated separately. The total water storage of the lake is then obtained by

237   summing the volumes of these three sections. Relying on R, lake boundary from Wang et al. (2020)

238   as well as DEM, m and n were estimated for GUL-1 and GUL-2 as shown in Table 3. In the case of

239   GCL-1, $l = m$ due to its small area of water surface. For GCL-2, m was determined as 35% of l for

240   lakes with $0.50 < R < 0.69$, 30% of l for lakes with $0.30 < R < 0.49$ and 20% of l for lakes with $R < 0.30$

241   (Table 3).

242   For GUL-1, R ranges from 0.50 to 0.10, both m and n are considered equal to half of l. On the

243   other hand, for GUL-2, it is possible to estimate the MDL water storage solely based on r, as

244   described in Equation 7. Accordingly, r values were statistically set up as $0.4l$, $0.55l$, and $0.65l$,

245   respectively with three R levels (Table 3). Figure 5 illustrates several representative cases of MDLs.

246   The above quantitative question about m, n and r is not based on subjective judgment. First,

247   we computed the R values for all glacial lakes utilizing catalog data, then categorized them by glacial

248   lake type, and finally, we provided a definition by statistically assessing the shape of glacial lakes.

249   This definition pertains to the proportionality of m, n, and r concerning the l of the glacial lake.

250   Consequently, our model is capable of autonomously classifying each glacial lake type through

251   boundary data analysis. It further computes various parameters for each lake, encompassing m, n, r,

252   and h, ultimately culminating in the determination of the water storage for each lake.

253   **Table 3** Quantification of model input parameters.

Lake type	Calculation rules of model input parameters					
	a	w, l	R	m	n	r
GCL-1			$0.70 \leq R \leq 1.0$	l	0	0
GCL-2	Median slope within the 80 m buffer zone outside the lake boundary	w is the diameter of the largest inscribed circle and l is the maximum length of the minimum bounding geometry	$0.50 \leq R \leq 0.69$	$l \times 0.35$	0	$l-m$
			$0.30 \leq R \leq 0.49$	$l \times 0.30$	0	$l-m$
			$0.10 \leq R \leq 0.29$	$l \times 0.20$	0	$l-m$
GUL-1			$0.50 \leq R \leq 1.0$	$l \times 0.50$	$l \times 0.50$	0
GUL-2			$0.40 \leq R \leq 0.49$			$l \times 0.40$
			$0.30 \leq R \leq 0.39$	$l-r$		$l \times 0.55$
			$0.10 \leq R \leq 0.29$			$l \times 0.65$

254
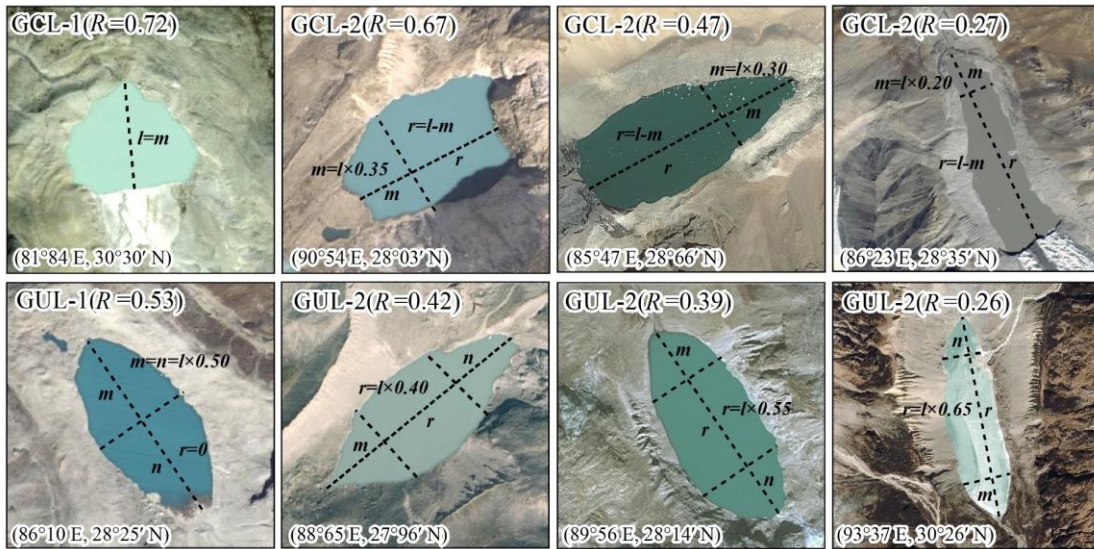
255

256   **Figure 5**. Example for the extraction of input parameters for different types of MDLs. The base map is a Google

257   Earth image (©Google Earth).

258   We executed our workflow (Figure 6) on 44 MDLs in High Mountain Asia that have known

259   depths and water storages. For each lake, we checked whether its outline was in contact to the parent

260   glacier. We automatically fitted a rectangular bounding box to calculate R, and then automatically

261   assigned each lake to one of the four types of MDL based on R thresholds (Table 1). Finally, we

262   estimated their water storages using our and traditional empirical relationships. Our model requires

263   MDL boundary and DEM data as inputs, and it automatically quantifies each parameter while

264   selecting the optimal model for water storage estimation.

265   Finally, we applied our model to more than 10,000 glacial lakes with unknown bathymetry in

266   High Mountain Asia. This region had one of the highest rates of MDLs growth in the world in past

267   decades.
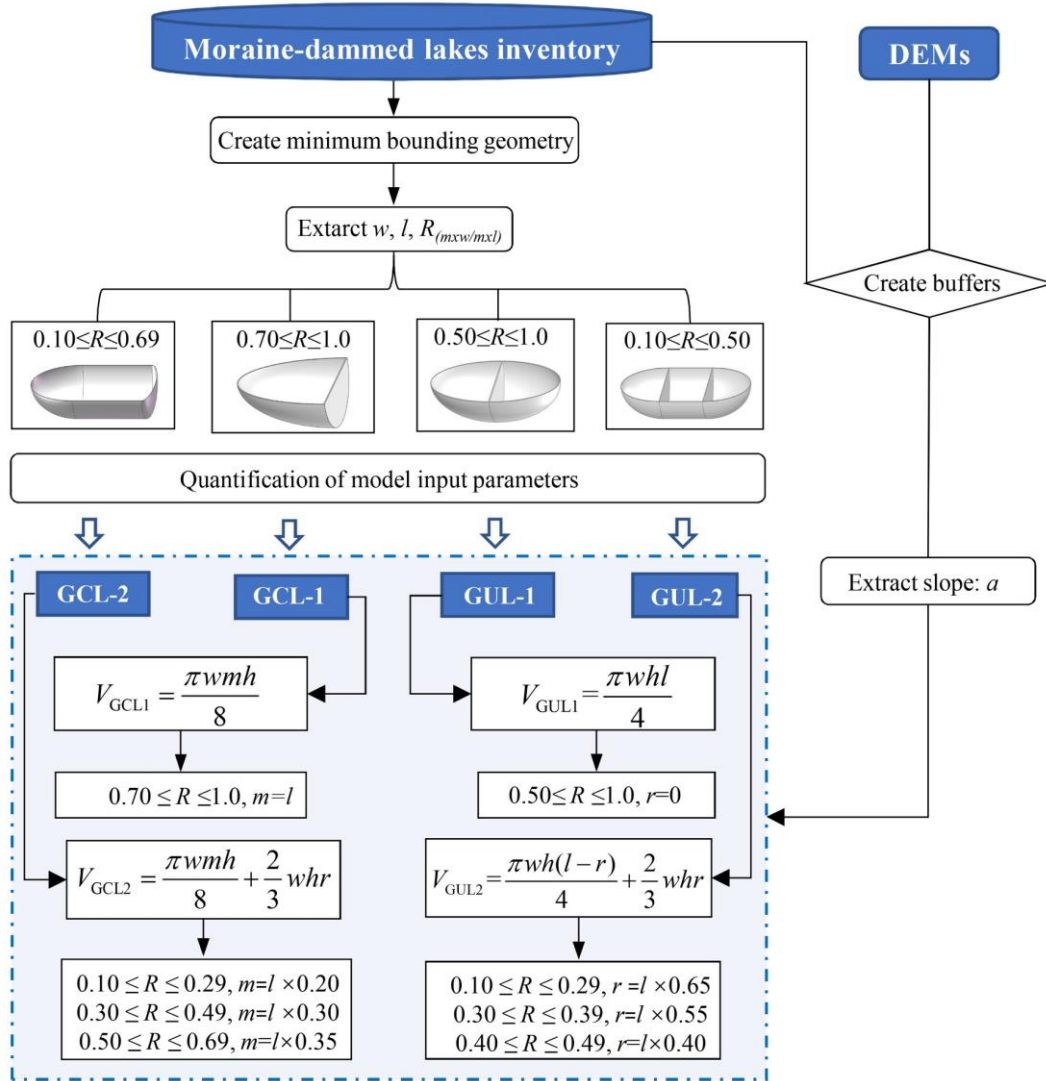
268

269   **Figure 6**. The flow chart of the model procedure derivation.

270   **3.4. Model validation and application**

271   In this study, we initially validated our parameterization using bathymetric measurements from

272   four representative glacial lakes surveyed between 2020 and 2021. Subsequently, we combined the

273   data from these four lakes with the remaining six glacier lakes we measured, along with water

274   storage data from 34 MDLs obtained from relevant literature sources (see Appendix A for details).

275   This resulted in a dataset of 44 lakes, which was used to compare and validate the performance of

276   our model against other existing methods.

277   A glacier lake inventory of the High Mountain Asia region, published by Wang et al, 2020 was

278   used as input data for the model application to assess the water storage of moraine-dammed lakes

279   in this region. Notably, Wang's glacier lake inventory provides a detailed classification of GCL and

280   GUL, which has been internationally recognized. It is important to note that in his dataset, GUL

281   refers specifically to glacier lakes that do not contact glaciers, which may not necessarily all be

282   moraine-dammed lakes. To ensure the accuracy of our analysis, we conducted a thorough review

283   based on the classification criteria proposed by Yao et al., (2018) which identify three types of

284   moraine-dammed lakes: (1) lakes situated between the end moraine ridge and the glacier terminus,

285   (2) lakes beside the lateral moraine ridge, and (3) lakes on the moraine ridge. Each GUL in the

286   dataset was individually assessed against these criteria, and only those meeting the classification as

287   moraine-dammed lakes were retained for further analysis.

288   **4. Results**

289   **4.1. Model validation**

290   We validated our parameterization using bathymetry measurements from four representative

291   glacial lakes, namely, Bienong Co, Maqiong Co, Tanong Co, and Jialong Co, located in the Qinghai-

292   Tibet Plateau. These lakes represent the four types of glacier lakes, with depths measured through

293   bathymetric surveying (Figure 7). In comparing estimated with measured water storages (Table 4),

294   we find that Jialong Co has the highest accuracy with a relative error of only 1%. Maqiong Co and

295   Tanong Co are overestimated by approximately 5% and 7%, respectively. The largest lake, Bienong

296   Co, had an underestimated water storage of 6%.

297   In addition, our model is designed to approximate the mean depth of MDLs and therefore

298   underestimates the maximum measured lake depth by about 50% (Table 4). Modeled mean water

299   depths only deviate by 18% (mean) from the measured mean water depths. Except for a notable

300   prediction error for Bienong Co (+47%), errors for Jialong Co, Tanong Co, and Maqiong Co range

301   from 6% to 13% relative to the measured values.

302   In summary, our model has a high degree of concordance with observed glacial lake water

303   storages and provides better estimations of water depth compared to the measured average depths.

304   This suggests that our proposed model can used in glacial lake water storage estimation and the

305 management of GLOF hazards.
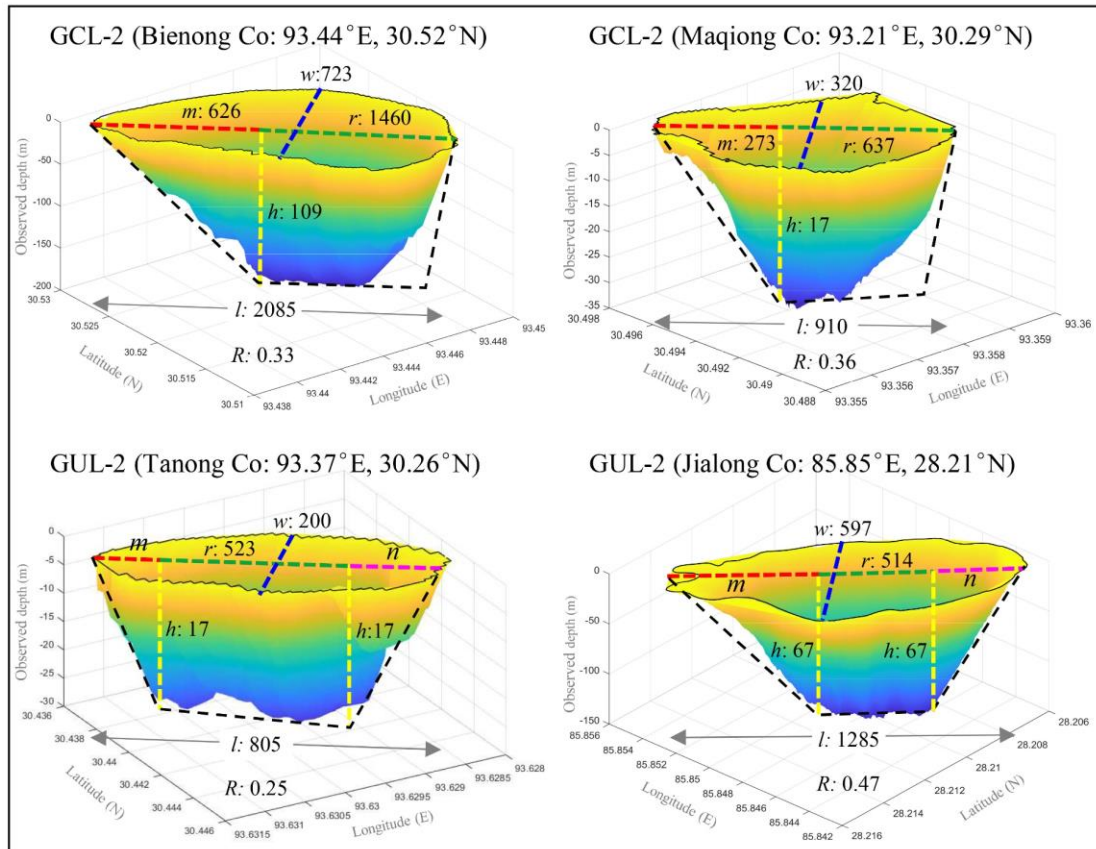
306

307 **Figure 7**. Subaqueous glacial lake morphology based on bathymetric surveys. The black dashed line represents the

308 hypothetical longitudinal profile of the glacial lake; *l* and *w* are measured from the lake boundary, *h* is simulated

309 lake depth and the remaining parameters (*m*, *n*, *r*) are calculated by rule in Table 3. Lake depth is exaggerated.

310 **Table 4** Validation results of the mathematical model.

Name	Year of survey	Type	Area (km^2)	Lake depth (m)			Water storage (10^6 m^3)		
				Observed (max/mean)	Simulated (mean)	Relative error	Observed	Simulated	Error
Bienong Co	2021	GCL2	1.16	181/74	109	+47%	102.00	95.689	-6%
Maqiong Co	2021	GCL2	0.22	34/16	17	+6%	3.325	3.581	+7%
Tanong Co	2021	GUL2	0.13	29/15	17	+13%	1.821	1.915	+5%
Jialong Co	2020	GUL2	0.55	135/62	67	+8%	37.530	37.952	+1%

311

312 **4.2. Comparison with other methods**

313 Table 5 displays the dataset of glacial lake bathymetry used in this study to validate the model.

314 We compared our model with another model that employed the lake geometry (Zhou et al., 2020),

315 and also with 20 additional formulas (EqS1-EqS20) collated by Qi et al. (2022) in Table S1. In the

316 estimation of a single MDL, formulas EqS4, EqS6, EqS13, EqS17, and EqS20 displayed significant

317   inaccuracies (132% - 853%). For instance, EqS13 shows an average error of 853%. Consequently,

318   we have refrained from conducting a comparative analysis of these five formulas in the subsequent

319   discussions.

320   **Table 5** The glacial lake bathymetry data set used in this study. The lake bathymetry data are shown in bold provided

321   by this study, and the rest are obtained from references, see Appendix A for details.

Lake Name	Type	Area (km^2)	Water storage(10^6m^3)		Measurements based on remote sensing images						
			Measured	Estimated	l	w	R	a	m	r	h
Kajiaqu	**GCL2**	**0.29**	**3.45**	**3.00**	**1436**	**230**	**0.13**	**14**	**287**	**1149**	**15**
Bienong Co	**GCL2**	**1.17**	**102.00**	**95.69**	**2085**	**723**	**0.33**	**31**	**626**	**1460**	**109**
Longmuqie Co	**GCL2**	**0.58**	**8.28**	**8.47**	**1775**	**380**	**0.21**	**12**	**355**	**1420**	**21**
Tanong Co	**GUL2**	**0.13**	**1.82**	**1.92**	**805**	**200**	**0.25**	**19**	**0**	**523**	**17**
Maqiong Co	**GCL2**	**0.22**	**3.32**	**3.58**	**910**	**320**	**0.36**	**12**	**273**	**673**	**17**
Zhasuo Co	**GUL2**	**0.33**	**4.28**	**5.18**	**890**	**380**	**0.4**	**12**	**0**	**356**	**21**
Jialong Co	**GUL2**	**0.55**	**37.53**	**37.95**	**1285**	**597**	**0.46**	**24**	**0**	**514**	**67**
Paqu Co	**GUL2**	**0.58**	**8.80**	**9.22**	**2134**	**314**	**0.15**	**14**	**0**	**1387**	**19**
Chmaqudan Co	**GUL2**	**0.56**	**19.61**	**17.91**	**1459**	**450**	**0.31**	**19**	**0**	**802**	**38**
Tara Co	**GUL2**	**0.23**	**2.64**	**3.19**	**1024**	**255**	**0.26**	**15**	**0**	**666**	**17**
Jialong Co	GUL2	0.46	18.20	18.59	1133	537	0.47	17	0	453	41
Rewuco	GCL1	0.42	13.85	8.52	839	613	0.73	15	839	0	42
PoiquNo.1	GCL2	0.09	2.53	2.21	428	300	0.64	22	150	278	30
Ranzeria Co	GCL2	0.29	3.88	3.16	1181	288	0.23	12	236	945	15
BethungTsho	GCL2	0.45	4.28	4.51	1355	373	0.28	9	271	1084	15
Guangxie Co	GCL2	0.41	2.61	2.71	1032	390	0.3	7	310	722	12
Shishapangma	GCL2	0.6	18.59	13.61	1721	500	0.29	12	344	1377	26
Lugge	GCL2	1.63	71.76	69.02	3163	578	0.18	23	633	2531	62
Raphstreng2	GCL2	1.31	58.19	59.13	2117	816	0.39	16	635	1482	59
Galong Co	GCL2	5.49	377.39	403.18	4284	1500	0.35	16	1285	2999	107
Bnecuoguo Co	GUL1	0.11	1.69	1.98	490	288	0.59	14	0	0	18
Cirenma Co	GUL2	0.33	12.43	12.03	1276	367	0.29	22	0	829	36
Longbasaba	GCL2	1.15	56.16	43.47	2114	680	0.3	17	634	1479	52
Midui	GCL2	0.22	1.13	1.34	968	280	0.31	7	290	678	8
Lugge	GCL2	1.18	58.30	39.18	2520	545	0.2	19	504	2016	47
Thulagi	GCL2	0.76	31.80	30.33	1991	437	0.22	28	398	1593	57
Tsho Rolpa	GCL2	1.39	76.60	62.59	2942	590	0.2	22	588	2353	59
Imja Tsho	GCL2	0.6	28.00	23.18	1341	543	0.38	22	402	939	54
Cirenma Co	GUL2	0.33	13.90	12.23	1276	370	0.29	22	0	829	37
Pidahu	GCL2	0.89	50.44	31.37	2071	500	0.21	22	414	1657	50
Imja Tsho	GCL2	1.14	63.80	52.55	2191	605	0.24	23	438	1753	65
South Lhonak	GCL2	1.31	65.80	71.22	2328	715	0.31	22	699	1630	73
Tam Pokhari	GCL2	0.45	21.25	26.02	1178	470	0.41	34	353	825	80
Thulagi	GCL2	0.91	23.30	31.83	2522	417	0.17	25	504	2017	49

Imja Tsho	GCL2	1.03	35.50	37.03	2028	556	0.27	21	406	1622	54
Thulagi	GCL2	0.94	35.37	36.19	2541	430	0.17	27	508	2033	54
Tsho Rolpa	GCL2	1.54	85.94	68.58	3304	566	0.17	23	661	2643	60
Thulagi	GCL2	0.92	36.10	37.75	2504	439	0.18	27	501	2003	56
Lower Barun	GCL2	2.14	103.60	111.38	3297	730	0.22	23	659	2638	76
Lower Barun	GCL2	1.77	112.30	97.45	3091	717	0.23	22	618	2473	72
Imja Tsho	GCL2	1.15	78.40	59.12	2208	610	0.24	25	442	1767	72
Amphulapche	GUL1	0.12	3.20	3.79	404	369	0.99	19	0	0	32
Chamlang Tsho	GCL2	0.76	35.00	26.53	1627	588	0.32	18	488	1139	47
Imja Tsho	GCL2	0.75	33.48	24.13	1557	550	0.32	19	467	1090	48

322  Our assessment (Table 6) involves the relative error (RE, absolute value), bias, root mean

323  square error (RMSE), mean absolute percentage error (MAPE) and mean absolute error (MAE) to

324  quantify the uncertainty of new model. We use the coefficient of determination R^2 to describe the

325  goodness of fit between the model-derived data series and the measured data. Accordingly, our

326  model had an R^2 value of approximately 0.98, indicating a strong correlation between observed and

327  predicted lake water storages (Figure 8). Moreover, our model has the lowest variance, according

328  to a bias (-0.0031 km^3), MAE (0.0059 km^3), RMSE (0.0096 km^3), and MAPE(25%). Also, our

329  model has the lowest average relative error, at around 14%. The average relative error of EqS2,

330  EqS3, EqS5, EqS7, EqS9, EqS11, EqS15 and EqS16 ranged from 44% to 50%, while the remaining

331  formulas display average relative errors exceeding 50%. Although all equations achieved $R^2 > 0.93$,

332  the predicted values have a high variance and tend to either overestimate or underestimate the water

333  storage of glacial lakes. Compared with our method, their bias, MAE, RMSE, and MAPE were all

334  55%, 64%, 52% and 64%, respectively, and thus higher than ours. EqS7 had a better prediction

335  accuracy. However, its bias, MAE and RMSE values are 82%, 64% and 52% higher than those of

336  our model, respectively. This indicates a significant estimation error for specific glacial lakes, and

337  both RMSE and MAE are sensitive to outliers. Overall, most of the equations tend to underestimate

338  glacial lake water storages, with the underestimation becoming more pronounced for larger water

339  storages. Nevertheless, we consider the accuracy level of our method to be acceptable due to the

340  lower uncertainty compared to other models, providing an alternative for predicting the water

341  storage of MDLs.

342
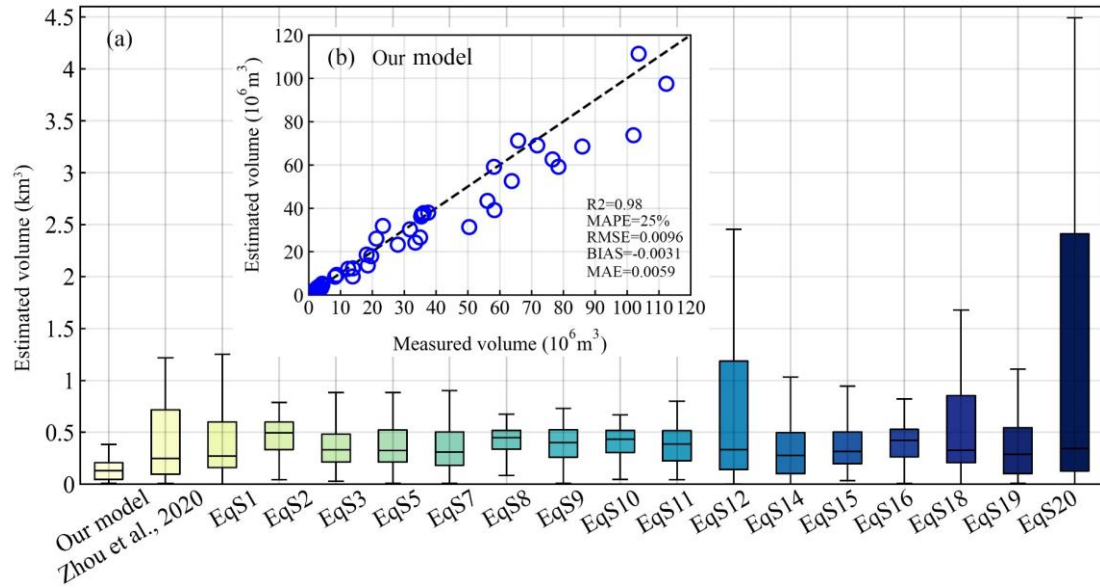
Figure 8. Comparison of the overall performance in glacial lake water storage estimation between our and previous models (a) and comparison of measured and estimated water storage by our model (b).

Table 6 Comparison of all empirical scaling relationships (EqS1-EqS20) in terms of bias, mean absolute error (MAE) and root mean square error (RMSE) are measured in cubic kilometers. See Appendix B for details.

Equation	RE	BIAS	MAE	MAPE	R²	RMSE
Our model	**14%**	**-0.0031**	**0.0059**	**25%**	**0.9793**	**0.0096**
Zhou et al., 2021	53%	0.0097	0.0142	95%	0.9289	0.0485
Eq1	63%	-0.0060	0.0104	49%	0.9654	0.0174
Eq2	49%	-0.0185	0.0192	130%	0.9521	0.0299
Eq3	50%	-0.0074	0.0100	44%	0.9556	0.0150
Eq4	164%	0.0448	0.0448	120%	0.9494	0.1035
Eq5	45%	-0.0056	0.0112	51%	0.9418	0.0182
Eq6	219%	0.0609	0.0609	130%	0.9509	0.1331
Eq7	48%	-0.0056	0.0097	41%	0.9516	0.0146
Eq8	52%	-0.0162	0.0177	117%	0.9621	0.0295
Eq9	49%	-0.0126	0.0143	74%	0.9556	0.0213
Eq10	50%	-0.0149	0.0164	98%	0.9596	0.0262
Eq11	49%	-0.0112	0.0131	63%	0.9551	0.0192
Eq12	94%	0.0089	0.0118	37%	0.9642	0.0186
Eq13	853%	0.2362	0.2362	159%	0.9590	0.4404
Eq14	51%	0.0022	0.0113	61%	0.9438	0.0268
Eq15	46%	-0.0048	0.0110	50%	0.9430	0.0182
Eq16	44%	-0.0153	0.0160	88%	0.9288	0.0230
Eq17	316%	0.2088	0.2089	292%	0.8736	0.7300
Eq18	77%	0.0178	0.0207	98%	0.9418	0.0582
Eq19	50%	0.0036	0.0124	74%	0.9379	0.0336

	Eq20	132%	0.000238	0.0132	59%	0.9501	0.0245

4.3. Application of the new model

Considering the frequent occurrence of GLOF events in High Mountain Asia, posing threats to downstream infrastructure and the safety of the lives and properties of the local communities, assessing the water storage of glacial lakes is crucial for management potentially hazardous ones (Nie et al., 2023). Therefore, this study employs our model to provide preliminary estimates of glacial lake water storages in the study area.

A glacial lake inventory data (Wang et al., 2020) reveals that in 2018, there were a total of 13,166 glacial lakes (≥ 0.01 km^2) distributed in High Mountain Asia. The dataset highlights a significant increase in both the number and area of GCLs from 1990 to 2018, experiencing a remarkable growth of 52% and 54%, respectively. Model estimation results indicate that the total glacial lake water storage in the study area was 37.18 km^3 in 2018. Over the past three decades, the overall MDL's water storage increased by 8.94 km^3 from 28.24 km^3 in 1990, representing a growth of approximately 32%. The expansion rates of glacial lakes varied significantly across different regions (Figure 9). Notably, the Hindu Kush-Karakoram and the central and eastern of the Himalayas to the Hengduan Mountains witnessed the fastest increases in both glacial lake area and water storage.
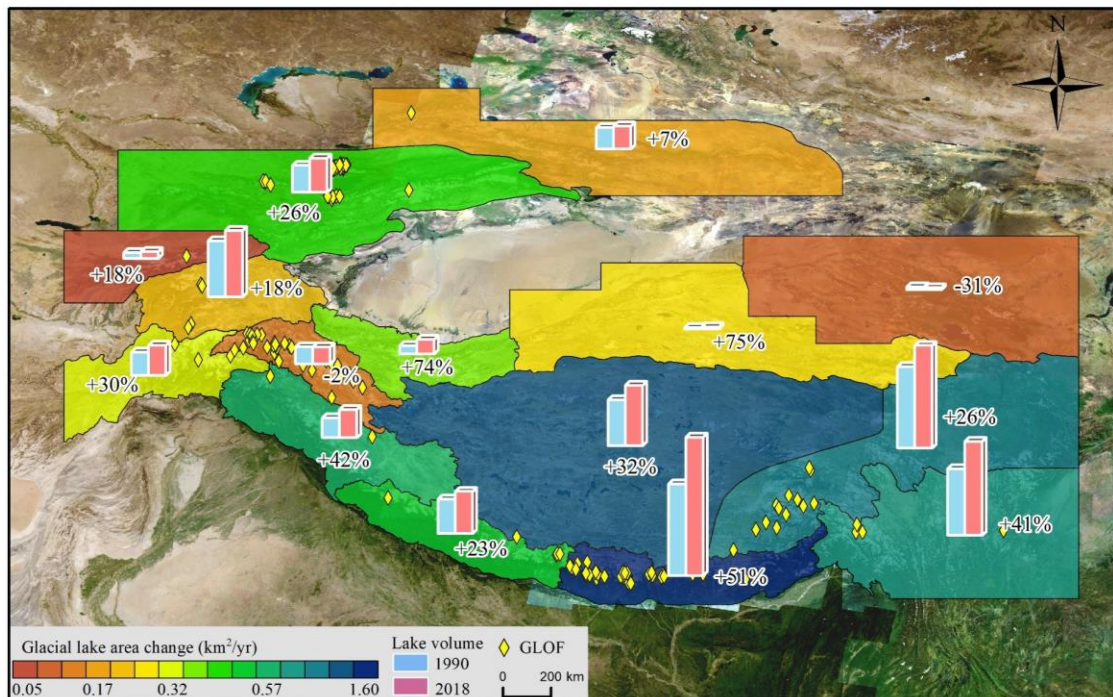
Figure 9 Changes in the area and water storage of glacial lakes from 1990 to 2018 in High Mountain Asia. The base

366   map is a Google Earth image (©Google Earth).

367   The Eastern Himalayas had the largest gain in both the area and water storage of glacial lakes,

368   concurrently establishing it as a hotspot for frequent GLOFs (Figure 9). The results indicate that the

369   water storage of 1,410 MDLs ($\geq$0.01 km^2) within the study area was $9,337 \pm 990 \times 10^6$ m^3 in 2022.

370   Among these, GCLs and GULs account for 70% and 30% of the total water storage, respectively.

371   Between 1990 and 2022, the total water storage in glacial lakes representing a substantial growth of

372   162%. Notably, GCLs contributed 134% with an average annual growth rate of 8.8% a^{-1}, indicating

373   an overall increase of 280%. In contrast, the change in the water storage of unconnected lakes

374   remained relatively stable, experiencing a modest growth of 52% over the past 32 years,

375   considerably lower than that of GCLs.

376   ## 5. Discussion

377   ### 5.1 Justification and uncertainty of model assumptions

378   In this study, we discuss the rationality and uncertainty of the model from three aspects. We

379   first assumed that the MDL features a parabolic longitudinal bottom profile and a uniformly

380   distributed sediment layer. The basin morphology of glacial lakes is a result of glacial erosion during

381   the glacier retreat process. Glacier erosion involves certain lateral shear stress, leading to the

382   formation of U-shaped valleys. Glacial lakes develop on these U-shaped valley terrains (Seddik et

383   al., 2009). Therefore, based on the lake bathymetry and the longitudinal bottom profile of the MDLs

384   (Figure 10), the variations in the underwater morphology of MDLs can be fitted with a parabolic

385   curve. However, when observing trends in underwater topography, it is evident that some large and

386   deep lakes (depth >100 m), such as Jialong Co and Bienong Co, exhibit relatively flat underwater

387   terrain, while others do not (Figure 7). This finding aligns with the research conducted by Carrivick

388   and Tweed (2013), who proposed that most proglacial lake basins have flat landforms resulting from

389   extensive sedimentation. These flat terrains, which were previously subdued and smoothed by

390   glaciation, can become covered and obscured by thin layers of silts and clays. Furthermore, it has

391   been suggested by some scholars that in large and deep proglacial lakes, the instability of the glacier

392   margin and the increased likelihood of wave erosion can lead to the erosion of moraine ridges at the

393   lake bottom (Murton et al., 2012).

394   The underwater landforms of some MDLs are not always a smooth parabolic shape. As

395   depicted in Figure 11, the bottom topography of most glacial lakes exhibits a fluctuating parabolic

396   trend. Golledge (2008) and Bennett et al. (2000) revealed that subaqueous moraines in glacial lakes

397   often have linear or sinuous crests, and their ridges frequently exhibit heavily glacitectonized

398   sediment structures indicative of compression. Although the presence of subaqueous moraines is

399   uncertain, this perspective offers a plausible explanation for the fluctuations in underwater

400   topography. In conclusion, concerning the formation process of subglacial geomorphology in MDLs

401   and lake bathymetry, both aspects substantiate our postulation that the MDL features a parabolic

402   longitudinal bottom profile. Furthermore, we hypothesize the presence of uniform sediment surface

403   to keep $h_1 = h_2$, although sediment distribution may be non-uniform due to factors such as the

404   position of the ice margin and water density (Carrivick and Tweed, 2013). As a result, the uneven

405   terrain at the bottom of some glacial lakes or the non-uniform distribution of sediments therein

406   constitutes one of the sources of uncertainty in the model.
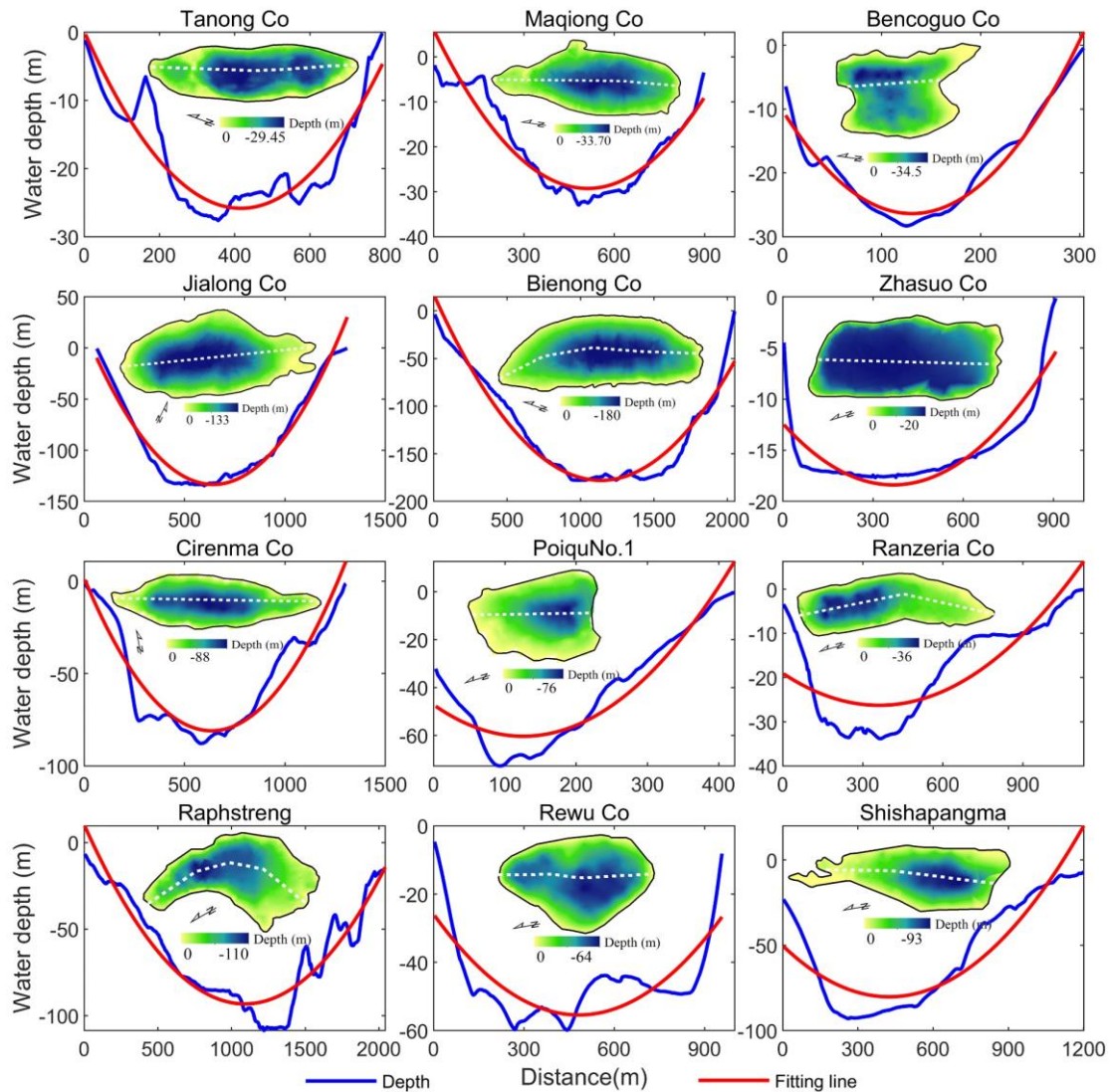
407

408   **Figure 10**. The longitudinal bottom profile underwater topography of the MDLs obtained by bathymetry and the

409   fitting lines of terrain change trend (The white dotted line is the longitudinal profile line of the lake).

410   The second source of uncertainty in the model arises from the assumption regarding the lake

411   surface of the MDL. Here, we assumed MDL's surface shape is characterized by an ellipse at both

412   ends and a rectangle in between. MDLs develop on parabolic or U-shaped glacial troughs. A mature

413   MDL, characterized by a relatively stable surface morphology, tends to exhibit an elliptical shape

414   due to its geological characteristics (e.g., GUL lake type in Figure 5). Similar trends in the

415   boundaries of MDLs are observed in different lake catalog datasets. Furthermore, in this study,

416   MDLs are classified into four types based on their geometric shapes (see Table 1). Treating the

417   complete geometric shape of an MDL as an ellipse allows the model to automatically partition the

418   lake basin structure (e.g., V_1, V_2, V_3 in Figure 2) based on the lake's shape coefficient, facilitating

419   the calculation of the water storage for MDLs with different morphologies. However, in reality, as

420   suggested by Teller (1987) and Rubensdotter et al. (2009), factors such as the position of the glacier

421   margin, surrounding landscape elevation and topography, and the location and elevation of lake

422   overflow channels can affect the basin morphology of MDLs. For instance, Bencoguo Co and

423   Raphstreng in Figure 10 do not exhibit the characteristic elliptical shape on the lake surface. This

424   uncertainty in the geometric shape of the lakes may lead to an overestimation of lake water storage

425   in the model, as the maximum width of the lake significantly influences the model results.

426   Finally, assuming the slope angle near the lake remains constant ($a=\beta$) is another aspect

427   contributing to the uncertainty in the model. In actuality, the slopes surrounding the lake exhibit

428   variations influenced by factors like the glacier tongue's position, the surrounding topography, and

429   the presence of moraine ridges. This variability in slope angles can further contribute to the

430   uncertainty when estimating the model's maximum water depth and water storage.

431   **5.2 Sensitivity of model input parameters**

432   Additionally, our model requires key parameters, namely, w, l, a, m, n, and r, with the

433   relationship between m, n, r, and l defined as $l = m + n + r$. Thus, we only investigated the sensitivity

434   of our model to l, w, and a. Since water depth is closely related to w and a (see equation (13)), we

435   also conducted parameter sensitivity tests on the estimated water depth using our model. In this

436   study, we employed Jialong Co and Bienong Co as representatives of GUL and GCL of MDLs,

437   respectively, to assess the sensitivity of the model to various parameters across different types of

438   glacial lakes. Figure 11 (a-f) demonstrates the sensitivity of volume (v) and water depth (h) in our

439   model to variations in the maximum length (*l*), maximum width (*w*), and slope (*a*) of glacial lakes.

440   Overall, there was a linear increase in glacial lake volume with changes in length (Figures11 a and

441   d). As shown in Figures 11b and e, variations in maximum width exhibited a consistent power-law

442   relationship with volume, where volume increased exponentially with width. The water depth of

443   glacial lakes demonstrated a linear increase with changes in width. The slope of the lake's edge

444   showed a power-law relationship with both estimated water depth and volume (Figures 11e and f).

445   In summary, when estimating volume using our model, glacial lake width and slope were found to

446   be the most sensitive parameters, followed by the lake's length. Regarding water depth, the model

447   was most sensitive to the slope, followed by the width.
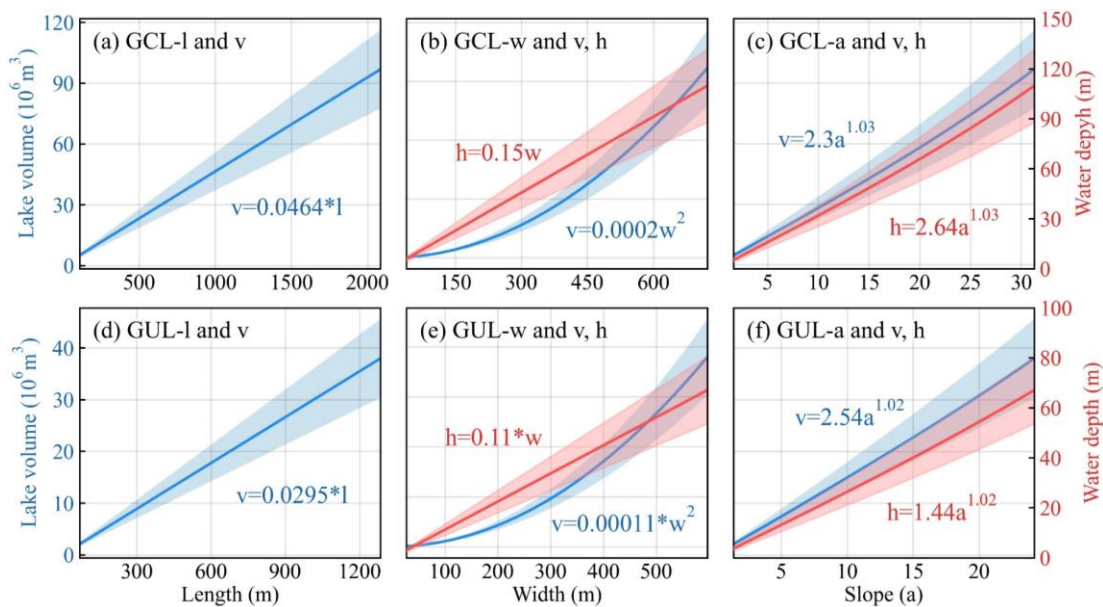
448

449   **Figure 11**. Parameter sensitivity analysis for glacial lake volume estimation using new model (note: the shaded
450   part represents the confidence interval, and definition of parameters in the figure as shown in Table 2).

6. Conclusion

452   Water storage plays a crucial role in predicting peak discharge of GLOFs. This study proposed

453   a mathematically robust and cost-effective approach for estimating lake water storage in regions

454   where field measurements of bathymetry are limited. The new model utilized lake geometry and

455   DEMs to estimate lake water storage. By parameterizing the model based on assumptions such as a

456   parabolic longitudinal bottom profile and consistent slope angles, it offers a reliable estimation of

457   lake water storage.

458   We validated our parameterization using bathymetry measurements from four representative

459   glacial lakes, namely, Bienong Co, Maqiong Co, Tanong Co, and Jialong Co, located in the Qinghai-

Tibet Plateau. Additionally, we applied the new model to 10 glacial lakes with depth measurements conducted during 2020-2021, and we included bathymetry data from 34 other glacial lakes sourced from published literature. Our model overcomes the autocorrelation issue inherent in earlier area/depth-water storage relationships and incorporates an automated calculation process based on the topography and geometrical parameters specific to MDLs. Compared to other models, our model achieved the lowest average relative error of approximately 14% when analyzing 44 observed data, surpassing the >44% average relative error from alternative models. This study model will allow researchers and practitioners to better predict potential outburst water storages and peak discharge of MDLs.

Competing interests

The contact author has declared that none of the authors has any competing interests.

Data availability

All data used in this study can be found in Table 5 and supplementary files.

Acknowledgments

This work was supported by research grants from the Second Tibetan Plateau Scientific Expedition and Research (Grant No.2019QZKK0208), the National Natural Science Foundation of China (No.42171129 and No.42361144874), the postdoctoral research start-up project of Yunnan Normal University (Grant No.01300205020503329).

References:

Bennett, M. R., Huddart, D., McCormick, T.: The glaciolacustrine landform–sediment assemblage at Heinabergsjökull, Iceland. Geogr Ann A., 82, 1–16, https://doi.org/10.1111/j.0435-3676.2000.00107.x, 2000.

Bolch, T., Kulkarni, A., Kääb, A., Huggel, C., Paul, F., Cogley, J. G., Frey, H., Kargel, J. S., Fujita, K., Scheel, M., Bajracharya, S., and Stoffel, M.: The state and fate of Himalayan glaciers, Science, 336, 310–314, https://doi.org/10.1126/science.1215828, 2012.

Carrivick, J. L., and Quincey, D.J.: Progressive increase in number and water storage of ice-marginal lakes on the western margin of the Greenland Ice Sheet, Global Planet Change, 116, 156–163, https://doi.org/10.1016/j.gloplacha.2014.02.009, 2014.

Carrivick, J. L., and Tweed, F. S.: Proglacial lakes: character, behaviour and geological importance, Quaternary Sci Rev., 78, 34–52, https://doi.org/10.1016/j.quascirev.2013.07.028, 2013.

490   Clague, J. J., and Evans, S. G.: A review of catastrophic drainage of moraine-dammed lakes in

491   British Columbia, Quaternary Sci Rev., 19, 1763–1783, https://doi.org/10.1016/S0277-

492   3791(00)00090-1, 2000.

493   Cook, K. L., Andermann, C., Gimbert, F., Adhikari, B. R., and Hovius, N.: Glacial lake outburst

494   floods as drivers of fluvial erosion in the Himalaya, Science, 362, 53–57,

495   https://doi.org/10.1126/science.aat4981, 2018.

496   Cook, S. J., and Quincey, D. J.: Estimating the volume of Alpine glacial lakes, Earth Surf. Dynam.,

497   3, 559–575, https://doi.org/10.5194/esurf-3-559-2015, 2015.

498   Duan, H., Yao, X., Zhang, Y., Jin, H., Wang, Q., Du, Z., Hu, J., Wang, B., and Wang, Q.: Lake water

499   storage and potential hazards of moraine-dammed glacial lakes–a case study of Bienong Co,

500   southeastern Tibetan Plateau, Cryosphere, 17, 591–616, https://doi.org/10.5194/tc-17-591-

501   2023, 2023.

502   Emmer, A. and Vilímek, V.: New method for assessing the susceptibility of glacial lakes to outburst

503   floods in the Cordillera Blanca, Peru, Hydrol. Earth Syst. Sci., 18, 3461–3479,

504   https://doi.org/10.5194/hess-18-3461-2014, 2014.

505   Fischer, M., Korup, O., Veh, G., and Walz, A.: Controls of outbursts of moraine-dammed lakes in

506   the greater Himalayan region, Cryosphere, 15(8), 4145–4163, https://doi.org/10.5194/tc-15-

507   4145-2021, 2021.

508   Fujita, K., Sakai, A., Takenaka, S., Nuimura, T., Surazakov, A. B., Sawagaki, T., and Yamanokuchi,

509   T.: Potential flood water storage of Himalayan glacial lakes, Nat. Hazards Earth Syst. Sci., 13,

510   1827–1839, https://doi.org/10.5194/nhess-13-1827-2013, 2013.

511   Gao, Y., Liu, S., Qi, M., Xie, F., Wu, K., and Zhu, Y.: Glacier-related hazards along the International

512   Karakoram Highway: status and future perspectives, Front. Earth Sci., 9, 611501,

513   https://doi.org/10.3389/feart.2021.611501, 2021.

514   Golledge, N. R., and Phillips, E.: Sedimentology and architecture of De Geer moraines in the

515   western Scottish Highlands, and implications for grounding-line glacier dynamics, Sediment

516   Geol, 208, 1–14, https://doi.org/10.1016/j.sedgeo.2008.03.009, 2008.

517   Harrison, S., Kargel, J. S., Huggel, C., Reynolds, J., Shugar, D. H., Betts, R. A., Emmer, A., Glasser,

518   N., Haritashya, U. K., Klimeš, J., and Reinhardt, L.: Climate change and the global pattern of

519   moraine-dammed glacial lake outburst floods, Cryosphere, 12, 1195–1209,

https://doi.org/10.5194/tc-12-1195-2018, 2021.

Liermann, S., Beylich, A. A., and Welden, A. V.: Contemporary suspended sediment transfer and accumulation processes in the small proglacial Sætrevatnet sub-catchment, Bødalen, western Norway, Geomorphology, 167, 91–101, https://doi.org/10.1016/j.geomorph.2012.03.035, 2012.

Liu, S., Wu, T., Wang, X., Wu, X., Yao, X., Liu, Q., Zhang, Y., Wei, J., and Zhu, X.: Changes in the global cryosphere and their impacts: A review and new perspective, Sci. Cold Arid. Reg., 12, 343–354, https://doi.org/10.3724/SP.J.1226.2020.00343, 2021.

Lützow, N., Veh, G., and Korup, O.: A global database of historic glacier lake outburst floods, Earth Syst Sci Data., 15, 2983–3000, https://doi.org/10.5194/essd-15-2983-2023, 2023.

Mergili, M., Pudasaini, S. P., Emmer, A., Fischer, J. T., Cochachin, A., and Frey, H.: Reconstruction of the 1941 GLOF process chain at Lake Palcacocha (Cordillera Blanca, Peru), Hydrol. Earth Syst. Sci., 24, 93–114, https://doi.org/10.5194/hess-24-93-2020, 2020.

Murton, D. K., and Murton, J. B.: Middle and Late Pleistocene glacial lakes of lowland Britain and the southern North Sea Basin, Quatern Int, 260, 115–142, https://doi.org/10.1016/j.quaint.2011.07.034, 2012.

Nie, Y., Deng, Q., Pritchard, H. D., Carrivick, J. L., Ahmed, F., Huggel, C., Liu, L., Wang, W., Lesi, M., Wang, J., Zhang, H., Zhang, B., Lü, Q., and Zhang, Y.: Glacial lake outburst floods threaten Asia's infrastructure, Sci Bull, 68, 1361–1365, https://doi.org/10.1016/j.scib.2023.05.035, 2023.

Qi, M., Liu, S., Wu, K., Zhu, Y., Xie, F. M., Jing, H. A., Gao, Y. P., and Yao, X. J.: Improving the accuracy of glacial lake water storage estimation: a case study in the Poiqu basin, central Himalayas, J. Hydrol., 610, 127973. https://doi.org/10.1016/j.jhydrol.2022.127973, 2022.

Qi, M., Liu, S., Gao, Y., Xie, F., Pan, X., Zhang, Z., Yao, X., Zhang, C., and Zhu, Y.: Water volume changes and assessment of potential outburst triggers for glacial lakes in the Nidu Zangbo basin,southeastern Tibet:a case study of Tanong Co, J. Glaciol. Geocryol, 45, 1205–1219. https://doi.org/10. 7522/j. issn. 1000-0240. 2023. 0092, 2023.

Richardson, S. D., and Reynolds, J. M.: An overview of glacial hazards in the Himalayas. Quat. Int., 65, 31–47, https://doi.org/10.1016/S1040-6182(99)00035-X, 2000.

Rounce, D. R., Hock, R., Maussion, F., Hugonnet, R., Kochtitzky, W., Huss, M., Berthier, E.,

Brinkerhoff, D., Compagno, L., Copland, L., Farinotti, D., Menounos, B., and McNabb, R. W.: Global glacier change in the 21st century: Every increase in temperature matters, Science, 379, 78–83, https://doi.org/10.1126/science.abo1324, 2023.

Rubensdotter, L., and Rosqvist, G.: Influence of geomorphological setting, fluvial-, glaciofluvial- and mass-movement processes on sedimentation in alpine lakes, Holocene, 19, 665–678, https://doi.org/10.1177/0959683609104042, 2009.

Sattar, A., Haritashya, U. K., Kargel, J. S., Leonard, G. J., Shugar, D. H., and Chase, D.V.: Modeling lake outburst and downstream hazard assessment of the Lower Barun Glacial Lake, Nepal Himalaya, J. Hydrol., 598, 126208, https://doi.org/10.1016/j.jhydrol, 2021.

Seddik, H., Greve, R., Sugiyama, S., and Naruse, R.: Numerical simulation of the evolution of glacial valley cross sections, Phys Rev D., 61, 210–211, https://doi.org/10.1103/PhysRevD.61.114016, 2009.

Shugar, D. H., Burr, A., Haritashya, U. K., Kargel, J. S., Watson, C. S., Kennedy, M. C., Bevington, A. R., Betts, R. A., Harrison, S., and Strattman, K.: Rapid worldwide growth of glacial lakes since 1990, Nat. Clim. Chang., 10, 939–945, https://doi.org/10.1038/s41558-020-0855-4, 2020.

Teller, J. T.: Proglacial lakes and the southern margin of the Laurentide Ice Sheet. In: Ruddiman, W.F., Wright, H.E. (Eds.), North America and Adjacent Oceans During the Last Deglaciation. The Decade of North American Geology. Geological Society of America, Boulder, CO, K3, pp. 39–69, 1987.

Veh, G., Korup, O., and Walz, A.: Hazard from Himalayan Glacier Lake Outburst Floods, PNAS, 117, 907–912, https://doi.org/10.1073/pnas.1914898117, 2019.

Veh, G., Korup, O., von Specht, S., Roessner, S., and Walz, A.: Unchanged frequency of moraine-dammed glacial lake outburst floods in the Himalaya, Nat. Clim. Chang., 9, 379–383, https://doi.org/10.1038/s41558-019-0437-5, 2019.

Veh, G., Lützow, N., Kharlamova, V., Petrakov, D., Hugonnet, R., and Korup, O.: Trends, breaks, and biases in the frequency of reported glacier lake outburst floods, Earth's Future, 10, e2021EF002426, https://doi.org/10.1029/2021EF002426, 2022.

Wang, X., Guo, X., Yang, C., Liu, Q., Wei, J., Zhang, Y., Liu, S., Zhang, Y., Jiang, Z., and Tang, Z.: Glacial lake inventory of high-mountain Asia in 1990 and 2018 derived from Landsat images, Earth Syst Sci Data., 12, 2169–2182, https://doi.org/10.5194/ESSD-12-2169-2020, 2020.

580 Westoby, M. J., Glasser, N. F., Brasington, J., Hambrey, M. J., Quincey, D. J., and Reynolds, J. M.:

581 Modelling outburst floods from moraine-dammed glacial lakes, Earth-sci Rev., 134, 137–159,

582 https://doi.org/10.1016/j.earscirev.2014.03.009, 2014.

583 Wu, G., Yao, T., Wang, W., Zhao, H., Yang, W., Zhang, G., Li, S., Yu, W., Lei, Y., and Hu, W.: Glacial

584 hazards on Tibetan Plateau and surrounding alpines, Bull Chin Acad Sci., 34, 1285–1292,

585 CNKI:SUN:KYYX.0.2019-11-012, 2019.

586 Yao, X. J., Liu, S. Y., Han, L., Sun, M. P., and Zhao, L. L.: Definition and classification system of

587 glacial lake for inventory and hazards study. J. Geogr. Sci., 28, 229–241,

588 https://doi.org/10.1007/s11442-018-1467-z, 2018.

589 Zhang, G., Bolch, T., Yao, T., Rounce, D. R., Chen, W., Veh, G., King, O., Allen, S. K., Wang, M.,

590 and Wang, W.: Underestimated mass loss from lake-terminating glaciers in the greater

591 Himalaya, Nat Geosci., 16, 333–338, https://doi.org/10.1038/s41561-023-01150-1, 2023.

592 Zheng, G., Allen, S. K., Bao, A., Ballesteros-Cánovas, J. A., Huss, M., Zhang, G., Li, J., Yuan, Y.,

593 Jiang, L., Yu, T., Chen, W., and Stoffel, M.: Increasing risk of glacial lake outburst floods from

594 future Third Pole deglaciation, Nat. Clim. Chang., 11, 411–417,

595 https://doi.org/10.1038/s41558-021-01028-3, 2021a.

596 Zheng, G., Mergili, M., Emmer, A., Allen, S., Bao, A., Guo, H., and Stoffel, M.: The 2020 glacial

597 lake outburst flood at Jinwuco, Tibet: causes, impacts, and implications for hazard and risk

598 assessment, Cryosphere, 15, 3159–3180, https://doi.org/10.5194/tc-2020-379, 2021b.

599 Zhou, L. X., Liu, J. K., and Li, Y. L.: Calculation method of mathematical model of the moraine

600 dammed lake storage capacity, Sci. Technol. Eng, 20, 9804–9809,

601 https://doi.org/10.3969/j.issn.1671-1815.2020.24.016, 2020.

602 Zhu, S., Liu, B., Wan, W., Xie, H., Fang, Y., Chen, X., and Hong, Y.: A new digital lake bathymetry

603 model using the step-wise water recession method to generate 3D lake bathymetric maps based

604 on DEMs. Water, 11, 1151, https://doi.org/10.3390/w11061151, 2019.